Chinese Chemical Letters 37 (2026) 111987

Contents lists available at ScienceDirect

Chinese Chemical Letters

journal homepage: www.elsevier.com/locate/cclet

1-Azaazulene constructs: Overcoming the weak fluorescence of azulene derivatives *via* S_1-S_0 transitions

Zijian Zhang[1], Fangxin Du[1], Lijia Liu[1], Yixiang Sun, Jie Xue*, Hanshen Xin*

School of Microelectronics, Shanghai Engineering Research Center for Integrated Circuits and Advanced Display Materials, Shanghai University, Shanghai 201800, China

ARTICLE INFO

Article history:
Received 3 June 2025
Revised 14 October 2025
Accepted 20 October 2025
Available online 21 October 2025

Keywords:
Azulene
1-Azaazulene
Photophysical properties
Boron difluoride complexes
Organic light-emitting diode

ABSTRACT

Azulene derivatives are promising for optoelectronics but suffer from weak fluorescence due to anti-Kasha behavior. This study designed and synthesized four asymmetric 1-azaazulene-based BF_2 complexes (Ph-NN, Ph-ON, Ca-NN, Py-NN) to explore their optoelectronic potential. Unlike azulene derivatives, which predominantly exhibit $S_2 \rightarrow S_0$ emission, 1-azaazulene constructs demonstrate effective S_1-S_0 transitions, resulting in enhanced fluorescence. Py-NN, incorporating a pyrrole group, achieved a remarkable photoluminescence quantum yield (PLQY) of 19.3 % at 560 nm, attributed to enhanced HOMO-LUMO orbital overlap with an oscillator strength (f) of 0.4973, resulting in a high radiative rate ($k_r = 9.51 \times 10^7\ s^{-1}$) and suppressed non-radiative decay ($k_{nr} = 0.40 \times 10^9\ s^{-1}$). OLEDs employing Py-NN as an emitter exhibited orange electroluminescence at 565 nm with a maximum external quantum efficiency (EQE) of 3.0 %. The results demonstrate that 1-azaazulene can serve as a versatile platform for developing efficient fluorescent materials with applications in optoelectronics.

© 2026 Published by Elsevier B.V. on behalf of Chinese Chemical Society and Institute of Materia Medica, Chinese Academy of Medical Sciences.

Azulene has emerged as a promising candidate for constructing advanced organic optoelectronic materials due to its unique optoelectronic properties [1–6]. In recent years, azulene-based materials have been extensively investigated in organic field-effect transistors (OFETs), solar cells, and other related applications [7–14]. As illustrated in Figs. 1a and b, the asymmetric frontier molecular orbitals (FMO) of azulene reduce electron repulsion between unpaired electrons, resulting in a narrow energy gap between its ground state (S_0) and first excited state (S_1). This reduced energy gap leads to a visible-range absorption band ($S_0 \rightarrow S_1$ transition), endowing azulene with its characteristic blue color [15–17]. Furthermore, the significant energy difference between S_1 and S_2 ($\Delta E(S_2\text{-}S_1) > 10{,}000\ cm^{-1}$) coupled with orbital asymmetry slows the non-radiative $S_2 \rightarrow S_1$ transition while enhancing the radiative $S_2 \rightarrow S_0$ pathway. This gives rise to the anti-Kasha fluorescence behavior observed in azulene [18,19]. However, this unique photophysical property also confines the fluorescence of azulene and its derivatives to the short-wavelength region with inherently weak emission intensities [20–25]. For example, the reported azulene-based BN-heteroaromatics exhibit photoluminescence quantum yield (PLQY) of less than 0.5 % (Fig. S1a in Supporting information) [24].

As illustrated in Fig. 1a, replacement of the CH moiety at the 1-position of azulene with a N atom yields its heteroanalog, 1-azaazulene. Density functional theory (DFT) calculations demonstrate that N substitution profoundly alters the electronic structure and FMO energetics (Fig. 1b). Compared to pristine azulene (HOMO/LUMO = −5.20/−1.82 eV, $E_{gap} = 3.38$ eV), 1-azaazulene exhibits stabilized HOMO (−5.93 eV) and LUMO (−2.16 eV) levels, with the bandgap widening to 3.77 eV due to a more pronounced stabilization of the HOMO level. Time-dependent DFT (TD-DFT) calculations reveal that while 1-azaazulene retains asymmetric frontier orbitals, the S_0-S_1 energy gap becomes substantially wider than that of the azulene. Notably, the reduced S_2-S_1 energy separation accelerates the non-radiative $S_2 \rightarrow S_1$ conversion compared to azulene, effectively suppressing the anti-Kasha $S_2 \rightarrow S_0$ radiative transition. Such changes in electronic structure and FMO energetics render 1-azaazulene a promising scaffold for designing Kasha-compliant fluorescent materials with red-shifted emission profiles compared to its quinoline isomer (Fig. S2 in Supporting information) [26–29].

Boron difluoride (BF_2) complexes represent a prominent class of luminescent materials [30–35]. The lone pair electrons on the N atom of 1-azaazulene enable effective coordination, making it an ideal ligand for constructing BF_2 complexes [36–40]. In this study,

* Corresponding authors.
E-mail addresses: xuejie@shu.edu.cn (J. Xue), inhanshen@shu.edu.cn (H. Xin).
[1] These authors contributed equally to this work.

https://doi.org/10.1016/j.cclet.2025.111987
1001-8417/© 2026 Published by Elsevier B.V. on behalf of Chinese Chemical Society and Institute of Materia Medica, Chinese Academy of Medical Sciences.

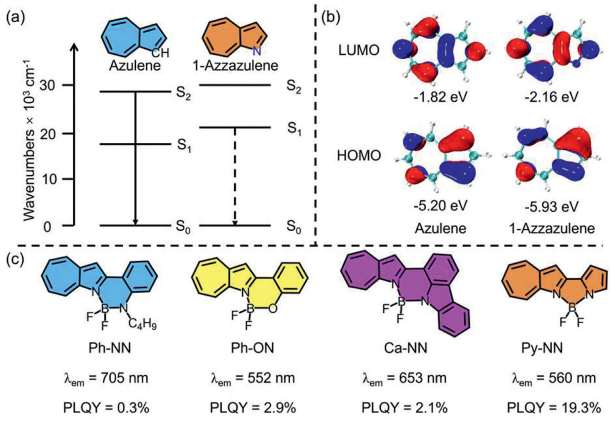
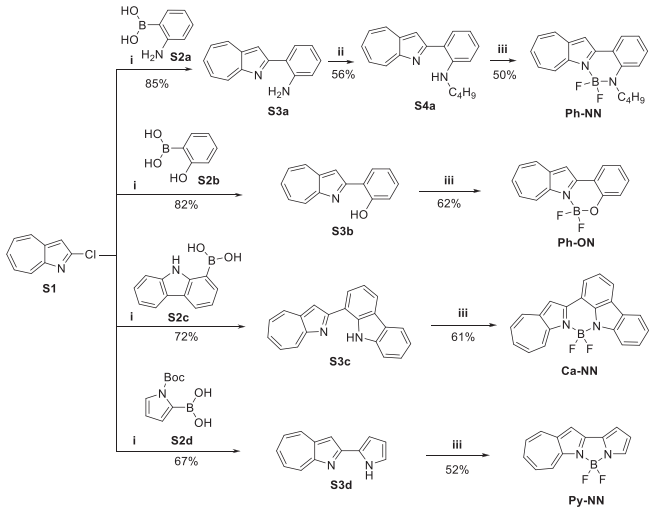


Fig. 1. (a) Chemical structures and schematic diagrams of radiation transitions for azulene and 1-azaazulene. (b) Frontier molecular orbitals and their energetics of azulene and 1-azaazulene. (c) Chemical structures, emission peaks, and photoluminescence quantum yields of the 1-azaazulene-based BF_2 complex.



Scheme 1. Synthesis route for Ph-NN, Ph-ON, Ca-NN, and Py-NN. (i) $Pd(PPh_3)_4$, K_2CO_3, THF, H_2O, 80–110 °C; (ii) C_4H_9Br, *n*-BuLi, THF, −78~35 °C; (iii) $BF_3{\cdot}Et_2O$, EtN_3/DIPEA, toluene, 35–80 °C.

four asymmetric 1-azaazulene-based BF_2 complexes (Ph-NN, Ph-ON, Ca-NN, and Py-NN, Fig. 1c) were designed, synthesized, and systematically investigated for their photophysical properties. The luminescence wavelength and efficiency of these complexes were modulated by structural variations in the ancillary coordination groups. In contrast to the anti-Kasha fluorescence observed in azulene derivatives, all four 1-azaazulene constructs display $S_1 \rightarrow S_0$ emission fluorescence. Ph-NN exhibits an emission peak at 705 nm, while Py-NN achieves a PLQY of 19.3 %. Furthermore, the organic light-emitting diode (OLED) fabricated with Py-NN as the emitter *via* a sensitization strategy delivers a maximum external quantum efficiency (EQE_{max}) of 3 %.

The synthetic routes for Ph-NN, Ph-ON, Ca-NN, and Py-NN are illustrated in Scheme 1. First, 2-chloro-1-azaazulene (**S1**) was synthesized according to the literature procedure [41,42]. Subsequently, Suzuki-Miyaura coupling reactions between **S1** and various arylboronic acids **S2a**-**S2d** were performed, affording intermediates **S3a**-**S3d** in 67 %-85 % yields. Notably, for reaction of **S1** and **S2d**, treatment with sodium methoxide during workup enabled *in situ* deprotection of the Boc group, directly affording intermediate **S3d**. To prevent potential interference of the amino group during BF_2 complex formation, **S3a** was substituted with an alkyl chain to

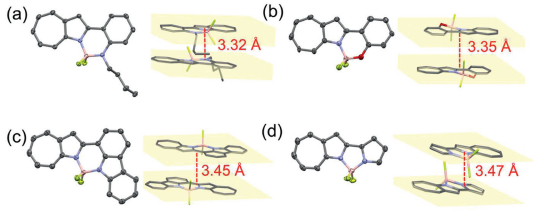


Fig. 2. Crystal structures and packing diagrams of (a) Ph-NN, (b) Ph-ON, (c) Ca-NN, and (d) Py-NN.

Table 1
Summarized key photophysical properties of compounds Ph-NN, Ph-ON, Ca-NN, and Py-NN.

Comp.	λ_{abs} (nm)[a]	λ_{em} (nm)[a]	Φ_{PL} (%)[a]	τ (ns)[a]	k_r (10^7 s^{-1})[b]	k_{nr} (10^9 s^{-1})[c]
Ph-NN	597	705	0.3	0.18	1.67	5.54
Ph-ON	487	552	2.9	0.84	3.45	1.16
Ca-NN	555	653	2.1	0.59	3.56	1.66
Py-NN	501	560	19.3	2.03	9.51	0.40

[a] Meassured in oxygen-free toluene solution (1×10^{-5} mol/L) at room temperature;
[b] Radiative rate constant is calculated as $k_r = \Phi_{PL}/\tau$;
[c] Non-radiative rate constant is calculated as $k_{nr} = (1 - \Phi_{PL})/\tau$.

obtain intermediate **S4a**. Finally, exposure of intermediates **S4a** and **S3b**-**d** to excess $BF_3{\cdot}Et_2O$ in toluene, in the presence of TEA/DIPEA, afforded 1-azaazulene-based BF_2 complexes Ph-NN, Ph-ON, Ca-NN, and Py-NN with 50 %-62 % yields. These compounds were characterized by nuclear magnetic resonance (NMR) spectroscopy and high-resolution mass spectrometry (HRMS). The full characterization data can be found in Supporting information.

The structures of Ph-NN, Ph-ON, Ca-NN, and Py-NN were further confirmed through X-ray single crystal analysis (Fig. 2, Tables S1-S4 in Supporting information). The single-crystal structures reveal that all four compounds possess highly planar backbones, with the largest dihedral angles in the fused rings being less than 4.95° (Fig. S3 in Supporting information). The crystal packing diagrams in Fig. 2 and Figs. S4-S7 (Supporting information) demonstrate that in Ph-NN, Ph-ON, Ca-NN, and Py-NN, adjacent molecules are arranged through antiparallel stacking of their conjugated backbones. The stacking distances, ranging from 3.32 Å to 3.47 Å, suggest that all four molecules have strong π-π interactions. These pronounced π-π interactions lead to a decrease in the PLQY of the thin films due to aggregation-caused quenching (ACQ) effects (Table S5 in Supporting information). As shown in Fig. S3, in the four BF_2 complexes, the average bond lengths (1.38–1.42 Å) of the 1-azaazulene and its connected aromatic rings are close to the bond length of aromatic C=C bonds, indicating that the ligand backbones maintain good aromaticity. The $NICS(1)_{zz}$ values (Fig. S8 in Supporting information) and the anisotropy of the induced current density (AICD) plots (Fig. S9 in Supporting information) further confirm the aromatic characteristics of the 1-azaazulene-based ligand backbones. Notably, the N→B coordination bonds in these four molecules (1.55–1.58 Å) are significantly shorter than those reported in asymmetric BF_2 complexes [43,44]. The short N→B bond lengths reflect strong dative interactions between nitrogen and boron, enhancing the complex's stability and ensuring the integrity of the fluorescent materials under various conditions.

To investigate the photophysical properties of Ph-NN, Ph-ON, Ca-NN, and Py-NN, we performed absorption spectroscopy, steady-state, and time-resolved emission spectroscopy under oxygen-free conditions at a concentration of 1×10^{-5} mol/L (Table 1). As shown in Fig. 3a, all four molecules exhibit intense absorption bands in the 300–400 nm range, primarily attributed to $S_0 \rightarrow S_2$ transi-

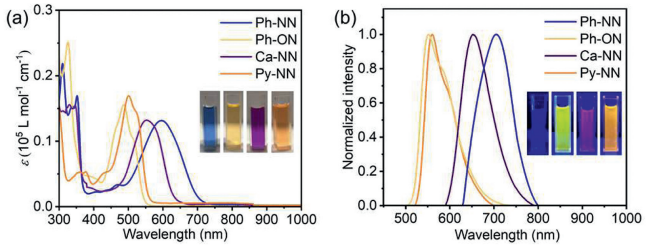


Fig. 3. (a) UV–vis absorption and (b) emission of compounds Ph-NN, Ph-ON, Ca-NN, and Py-NN (10^{-5} mol/L in oxygen-free toluene) with pictures inserted.

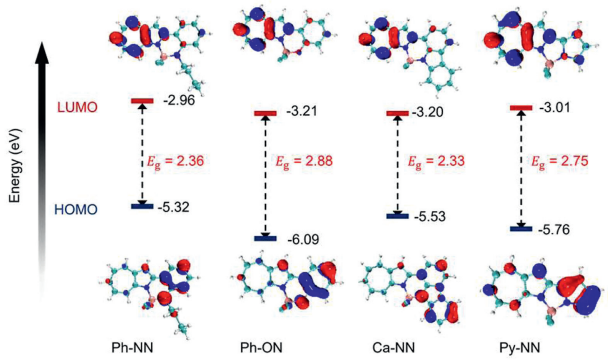


Fig. 4. Frontier molecular orbitals, and their energetics of compounds Ph-NN, Ph-ON, Ca-NN, and Py-NN, obtained by DFT and TD-DFT calculations.

tions of 1-azaazulene units. However, they exhibit distinct absorption differences in the long-wavelength region. Ph-ON and Py-NN display maximum absorption peaks at 487 and 501 nm, respectively, with pronounced shoulder peaks, indicating dominant localized excitations. In contrast, Ph-NN and Ca-NN show significantly red-shifted absorption at 597 and 555 nm, accompanied by broader absorption bands lacking distinct shoulders, which suggests excitations with pronounced charge-transfer (CT) characteristics. Notably, these absorption bands display significant redshifts compared to analogous quinoline derivatives [43,45,46], which may originate from the asymmetric electron distribution and narrower FMO energy gaps of the 1-azaazulene core. Remarkably, the molar absorption coefficients for the $S_0 \rightarrow S_1$ transitions of these compounds ($\varepsilon > 10^4$ L mol^{-1} cm^{-1}) are substantially higher than those of typical azulene-based molecules ($\varepsilon < 10^4$ L mol^{-1} cm^{-1}).

As depicted in Fig. 3b, Ph-NN exhibits an $S_1 \rightarrow S_0$ emission peak at 705 nm, a rare feature among small-molecule BF_2 complexes, with a Stokes shift (S) of 108 nm. However, its PLQY is only 0.3 %, likely due to ultrafast nonradiative decay. Time-resolved emission spectroscopy (Fig. S10a in Supporting information) reveals an exceptionally short luminescence lifetime (τ) of 0.18 ns for Ph-NN, yielding a radiative transition rate (k_r) of 1.67×10^7 s^{-1} and a nonradiative rate (k_{nr}) of 5.54×10^9 s^{-1} (Table 1). In contrast, Ph-ON and Ca-NN display blue-shifted emission peaks at 552 nm ($S = 74$ nm) and 653 nm ($S = 98$ nm), with improved PLQYs of 2.9 % and 2.1 %, respectively. Their luminescence lifetimes increase to 0.84 ns (Ph-ON) and 0.59 ns (Ca-NN), corresponding to k_r/k_{nr} values of 3.45×10^7 s^{-1}/1.16×10^9 s^{-1} and 3.56×10^7 s^{-1}/1.66×10^9 s^{-1} (Figs. S10b and c in Supporting information). Their enhanced PLQYs arise from both increased k_r and reduced k_{nr}. Significantly, Py-NN demonstrates the highest luminescence efficiency among the four 1-azaazulene-based BF_2 complexes, exhibiting an emission peak at 560 nm ($S = 59$ nm) with a PLQY of 19.3 %. The relatively small Stokes shift and high emission efficiency suggest dominant localized-state emission in Py-NN. Time-resolved photoluminescence spectrum (Fig. S10d in Supporting information) confirms a prolonged luminescence lifetime of 2.03 ns, corresponding to $k_r = 9.51 \times 10^7$ s^{-1} and $k_{nr} = 0.40 \times 10^9$ s^{-1}. These results indicate that by altering the structure of the groups attached to the 1-azaazulene, it is possible to tune the photophysical properties including absorption spectrum, emission spectrum, and emission efficiency of 1-azaazulene-based BF_2 complexes.

DFT calculations at the B3LYP/6–31G+(d,p) level were employed to investigate the electronic properties of the four 1-azaazulene-based BF_2 complexes, with the calculated data summarized in Table S6 (Supporting information). As illustrated in Fig. 4, the FMO of Ph-NN, Ph-ON, Ca-NN, and Py-NN exhibit significantly uneven electron density distributions, a notable contrast to most BF_2 complexes [47–49]. Specifically, the LUMO electron density is primarily distributed over the 1-azaazulene unit, while the HOMO electron density is mainly localized on the aniline, phenol, carbazole, and pyrrole moieties. For Ph-ON and Py-NN, especially the latter, the HOMO electron density also has a small distribution on the 1-azaazulene. This pronounced asymmetry in molecular orbital distribution suggests a propensity for charge-transfer (CT) transition absorption in these compounds, while Ph-ON and Py-NN may also exhibit localized transition absorption. As shown in Fig. 4, the calculations indicate that by altering the structure of the group connected to the 1-azaazulene, the FMO energetics and band gap of the 1-azaazulene-based BF_2 complexes can be effectively modulated, thereby tuning the absorption and emission wavelengths of the molecules.

Since the B3LYP functional may underestimate the energy of charge-transfer electronic states [50], the long-range corrected M062X functional was employed to study the excited states of 1-azaazulene-based BF_2 complexes using the 6–31G(d) basis set. TD-DFT calculations show that the oscillator strengths (f) for the $S_0 \rightarrow S_1$ transition of Ph-NN, Ph-ON, Ca-NN, and Py-NN are 0.3299, 0.3009, 0.3458, and 0.4973, respectively. The increased f could originate from the superior hole-electron overlap of S_1 state of Py-NN compared with the other three molecules. This indicates that Py-NN likely exhibits accelerated radiative decay rate (k_r). In addition, Py-NN demonstrated a relatively large energy gap ($\Delta E = 2.75$ eV) and smallest reorganization energy ($\lambda_M = 3942$ cm^{-1}), which is conducive to decelerating nonradiative decay rate (see Supporting information for details). Accordingly, Py-NN with large k_r and small k_{nr} likely exhibits high PLQY, which agrees well with the experimental results. In the electron-hole overlap maps of the S_1 excited state and atomic transition density matrix (TDM) heat maps for the $S_0 \rightarrow S_1$ transition (Fig. S10e in Supporting information), Ph-ON and Py-NN show substantial electron-hole overlap, primarily localized on the 1-azaazulene unit. This localization is favorable for the formation of localized excited states (LE). Additionally, the maps demonstrate that the electronic excitation process is chiefly focused on electron transfer among the atoms within the 1-azaazulene unit.

Cyclic voltammetry (CV) and differential pulse voltammetry (DPV) tests were performed on Ph-NN, Ph-ON, Ca-NN, and Py-NN, as shown in Figs. S11a-d and Table S8 (Supporting information). Electrochemical calculations determined the HOMO/LUMO levels of Ph-NN, Ph-ON, Ca-NN, and Py-NN to be −5.39/−3.61 eV, −6.39/−3.57 eV, −5.42/−3.70 eV, and −5.73/−3.63 eV, respectively. Overall, the FMO energy levels obtained from electrochemical measurements, particularly the HOMO levels, were consistent with the theoretical computational trends. Additionally, thermogravimetric analysis (TGA) was conducted and the results indicated that the thermal decomposition temperatures (T_d) for Ph-NN, Ph-ON, Ca-NN, and Py-NN were 273, 246, 371, and 428 °C (Fig. S12 in Supporting information), respectively, demonstrating good thermal stability across all compounds.

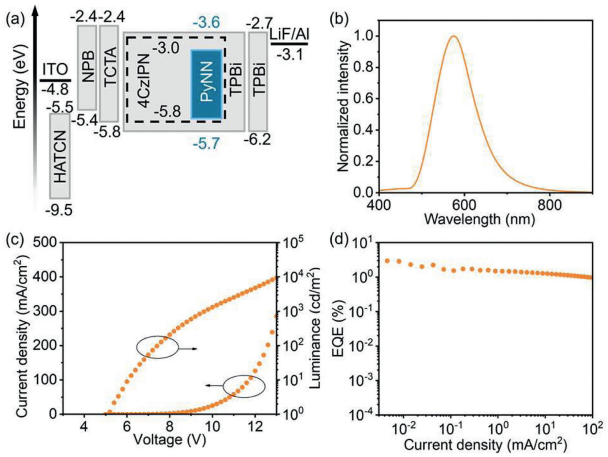


Fig. 5. (a) OLED device architecture. (b) Electroluminescent emission spectrum at 6 V. (c) The *J*–*V*–*L* (current density–voltage–luminance) characteristics. (d) The EQE–*J* (external quantum efficiency–current density) relationship.

Owing to the moderate PLQY and superior thermal stability of Py-NN, OLED devices were fabricated to evaluate the electroluminescent performance of 1-azaazulene-based BF_2 complexes with multilayer configurations of ITO/HATCN (5 nm, hole injection layer)/NPB (40 nm, hole-transport layer)/TCTA (10 nm, exciton-blocking layer)/TPBi: 20 wt% thermally activated delayed fluorescence sensitizer 4CZIPN and 1 wt% Py-NN (30 nm, emissive layer)/TPBi (25 nm, electron-transport layer)/LiF (1 nm, electron-injection layer)/Al (150 nm) (Fig. 5a and Fig. S12). As shown in Fig. 5b, the device exhibits strong orange emission with the corresponding electroluminescence peak value (λ_{em}) located at 565 nm, which is close to the photoluminescnece peak of Py-NN. And the OLED exhibited an EQE_{max} of 3.0 % and a turn-on voltage of 5.2 V.

In summary, this study successfully designed and synthesized four asymmetric 1-azaazulene-based BF_2 complexes (Ph-NN, Ph-ON, Ca-NN, and Py-NN) to explore their optoelectronic properties. By modifying ancillary coordination groups, the FMO energetics and band gaps of these complexes were effectively tuned, allowing adjustments in their absorption and emission properties. All four 1-azaazulene constructs exhibit $S_1 \rightarrow S_0$ emission fluorescence, in contrast to azulene derivatives, which typically display anti-Kasha fluorescence and low PLQY. Notably, Py-NN demonstrated superior performance, achieving a PLQY of 19.3 % with an emission peak at 560 nm. This enhancement is attributed to improved HOMO-LUMO overlap and suppressed nonradiative decay pathways. OLEDs incorporating Py-NN as an emissive dopant exhibited a maximum EQE of 3 %, underscoring its electroluminescent potential. These findings demonstrate that 1-azaazulene serves as a promising scaffold for developing fluorescent materials, overcoming the inherent limitations of traditional azulene derivatives and advancing its potential applications in optoelectronic devices. Moreover, 1-azaazulene constructs possess smaller band gaps compared to traditional fluorescent materials with similar-sized π-conjugated systems. This characteristic facilitates the development of long-wavelength emission fluorescent materials, which are desirable for applications requiring deep-red or near-infrared emission.

Declaration of competing interest

The authors declare that they have no known competing financial interests or personal relationships that could have appeared to influence the work reported in this paper.

CRediT authorship contribution statement

Zijian Zhang: Writing – original draft, Formal analysis, Data curation. **Fangxin Du:** Writing – original draft, Methodology, Formal analysis. **Lijia Liu:** Formal analysis, Data curation. **Yixiang Sun:** Formal analysis. **Jie Xue:** Writing – review & editing, Methodology, Investigation. **Hanshen Xin:** Writing – review & editing, Writing – original draft, Project administration, Investigation, Funding acquisition, Conceptualization.

Acknowledgments

This research was financially supported by the Natural Science Foundation of Shanghai Municipality (No. 25ZR1402168), the National Natural Science Foundation of China (No. 22101170) and Shanghai University. We thank Wen-wen Zhang and Jinheng Pan (Mass Spectrometry & Metabolomics Core Facility of Westlake University) for MS analysis.

Supplementary materials

Supplementary material associated with this article can be found, in the online version, at doi:10.1016/j.cclet.2025.111987.

References

[1] A. Ong, T. Tao, Q. Jiang, et al., Angew. Chem. Int. Ed. 61 (2022) e202209286.
[2] H. Xin, B. Hou, X. Gao, Acc. Chem. Res. 54 (2021) 1737–1753.
[3] J. Huang, S. Huang, Y. Zhao, et al., Small Methods 4 (2020) 2000628.
[4] J.X. Dong, H.L. Zhang, Chin. Chem. Lett. 27 (2016) 1097–1104.
[5] Y. He, Y. Zhu, M. Luo, H. Xia, Chin. Chem. Lett. 36 (2025) 110463.
[6] B. Yu, P. Du, J. Guo, H. Xin, J. Zhang, Chin. Chem. Lett. 35 (2024) 109321.
[7] L. Zhou, F. Qiu, Y. Ding, et al., Angew. Chem. Int. Ed. 63 (2024) e202409750.
[8] H. Xin, C. Ge, X. Jiao, et al., Angew. Chem. Int. Ed. 57 (2017) 1322–1326.
[9] M. Murai, S. Iba, S. Hamao, et al., Bull. Chem. Soc. Jpn. 96 (2023) 1077–1081.
[10] J. Wen, F. du, B. Yu, Chem. Sci. 15 (2024) 12589–12597.
[11] H. Nishimura, N. Ishida, A. Shimazaki, et al., J. Am. Chem. Soc. 137 (2015) 15656–15659.
[12] C. Zhang, Y. Kong, J. Xiang, et al., Chem. Sci. 16 (2025) 1353–1363.
[13] G. Yang, S. Sangtarash, Z. Liu, et al., Chem. Sci. 8 (2017) 7505–7509.
[14] X. Fu, H. Han, D. Zhang, et al., Chem. Sci. 11 (2020) 5565–5571.
[15] M. Beer, H.C. Longuet-Higgins, J. Chem. Phys. 23 (1955) 1390–1391.
[16] M. Kasha, Discuss. Faraday Soc. 9 (1950) 9–14.
[17] J. Michl, E.W. Thulstrup, Tetrahedron 32 (1976) 205–209.
[18] D. Dunlop, L. Ludvíková, A. Banerjee, H. Ottosson, T. Slanina, J. Am. Chem. Soc. 145 (2023) 21569–21575.
[19] R. Pino-Rios, R. Báez-Grez, D.W. Szczepanik, M. Solá, Phys. Chem. Chem. Phys. 26 (2024) 15386–15392.
[20] N. Tetreault, R.S. Muthyala, R.S.H. Liu, R.P. Steer, J. Phys. Chem. A 103 (1999) 2524–2531.
[21] H. Yamaguchi, S. Sato, M. Yasunam, T. Sato, M. Yoshinobu, Spectrochim. Acta A 53 (1997) 2471–2473.
[22] O.K. AbouZied, H.K. Sinha, R.P. Steer, J. Mol. Spectrosc. 183 (1996) 42–56.
[23] H. Yamaguchi, S. Sato, M. Yasunam, T. Sato, M. Yoshinobu, Spectrochim. Acta A 53 (1997) 2471–2473.
[24] H. Xin, J. Li, X. Yang, X. Gao, J. Org. Chem. 85 (2019) 70–78.
[25] J. Zhao, H. Huang, N. Li, et al., Tetrahedron 144 (2023) 133581.
[26] S.H. El-Demerdash, S.A. Halim, A.M. El-Nahas, A.B. El-Meligy, Sci. Rep. 13 (2023) 15626.
[27] S.A. Halim, A.B. El-Meligy, A.M. El-Nahas, S.H. El-Demerdash, Sci. Rep. 14 (2024) 219.
[28] A.B. El-Meligy, S.H. El-Demerdash, M.A. Abdel-Rahman, et al., ACS Omega 7 (2022) 14222–14238.
[29] Y.Q. Zhang, C.C. Yang, J.Y. Ma, W.Q. Tian, Chem. Sci. 15 (2024) 2100–2111.
[30] A. Loudet, K. Burgess, Chem. Rev. 107 (2007) 4891–4932.
[31] D. Wang, X. Wang, S. Zhou, et al., Coord. Chem. Rev. 482 (2023) 215074.
[32] M. Poddar, R. Misra, Coord. Chem. Rev. 421 (2020) 213462.
[33] G. Ulrich, R. Ziessel, A. Harriman, Angew. Chem. Int. Ed. 47 (2008) 1184–1201.
[34] Z. Shi, X. Han, W. Hu, et al., Chem. Soc. Rev. 49 (2020) 7533–7567.
[35] J. Wang, Q. Gong, L. Jiao, E. Hao, Coord. Chem. Rev. 496 (2023) 215367.
[36] X. Shao, M. Liu, J. Liu, L. Wang, Angew. Chem. Int. Ed. 61 (2022) e202205893.
[37] J. Wakabayashi, M. Gon, K. Tanaka, Y. Chujo, Macromolecules 53 (2020) 4524–4532.
[38] Y. Cao, C. Zhu, M. Barłóg, et al., J. Org. Chem. 86 (2021) 2100–2106.
[39] M. Zhao, Z. Yuan, Y. Zhou, Org. Lett. 26 (2024) 8837–8841.
[40] F. Yang, F. Ren, X. Liu, M. Zhao, Y. Zhou, Asian J. Org. Chem. 14 (2025) e202400804.
[41] T. Nozoe, S. Seto, S. Matsumura, T. Asano, Proc. Jpn. Acad. 32 (1956) 339–343.

[42] K. Yukio, K. Masaji, J. Am. Chem. Soc. 79 (1957) 5460–5463.
[43] T. Nakano, A. Sumida, K. Naka, J. Org. Chem. 86 (2021) 5690–5701.
[44] M. Zhao, F. Ren, Y. Zhou, Chem. Eur. J. 30 (2024) e202401784.
[45] K. Yamamoto, S. Matsui, S.I. Kato, Y. Nakamura, Org. Biomol. Chem. 21 (2023) 5398–5405.
[46] R.Z. Ma, Q.C. Yao, X. Yang, M. Xia, J. Fluorine Chem. 137 (2012) 93–98.
[47] L. Gai, J. Mack, H. Lu, et al., Chem. Eur. J. 20 (2013) 1091–1102.
[48] H. Liu, H. Lu, J. Xu, et al., Chem. Commun. 50 (2014) 1074–1076.
[49] H. Lu, J. Mack, Y. Yang, Z. Shen, Chem. Soc. Rev. 43 (2014) 4778–4823.
[50] J.L. Bredas, Chem. Mater. 29 (2017) 477–478.